

Intermediate degrees of synergistic pleiotropy drive adaptive evolution in ecological time

Léa Frachon¹, Cyril Libourel¹, Romain Villoutreix², Sébastien Carrère¹, Cédric Glorieux², Carine Huard-Chauveau¹, Miguel Navascués^{3,4}, Laurène Gay⁵, Renaud Vitalis^{3,4}, Etienne Baron², Laurent Amsellem², Olivier Bouchez^{6,7}, Marie Vidal^{6,8}, Valérie Le Corre⁹, Dominique Roby¹, Joy Bergelson¹⁰ and Fabrice Roux^{1,2*}

Rapid phenotypic evolution of quantitative traits can occur within years, but its underlying genetic architecture remains uncharacterized. Here we test the theoretical prediction that genes with intermediate pleiotropy drive adaptive evolution in nature. Through a resurrection experiment, we grew *Arabidopsis thaliana* accessions collected across an 8-year period in six micro-habitats representative of that local population. We then used genome-wide association mapping to identify the single-nucleotide polymorphisms (SNPs) associated with evolved and unevolved traits in each micro-habitat. Finally, we performed a selection scan by testing for temporal differentiation in these SNPs. Phenotypic evolution was consistent across micro-habitats, but its associated genetic bases were largely distinct. Adaptive evolutionary change was most strongly driven by a small number of quantitative trait loci (QTLs) with intermediate degrees of pleiotropy; this pleiotropy was synergistic with the per-trait effect size of the SNPs, increasing with the degree of pleiotropy. In addition, weak selection was detected for frequent micro-habitat-specific QTLs that shape single traits. In this population, *A. thaliana* probably responded to local warming and increased competition, in part mediated by central regulators of flowering time. This genetic architecture, which includes both synergistic pleiotropic QTLs and distinct QTLs within particular micro-habitats, enables rapid phenotypic evolution while still maintaining genetic variation in wild populations.

Contemporary and rapid phenotypic evolution has been observed in many natural populations of plant and animal species^{1,2}, especially during invasion³ and in response to both global climate change⁴ and toxic pollution⁵. A handful of studies have identified the genetic architecture of contemporary adaptive evolution of qualitative traits (such as industrial melanism)⁶ or single quantitative traits (such as herbicide detoxification in weeds or heavy-metal tolerance)^{7,8}. However, the genetic architecture of many traits simultaneously experiencing contemporary adaptive evolution, especially assayed at the level of whole genomes, remains unexplored, despite its importance for predicting evolutionary trajectories of natural populations^{9,10}.

There are many factors that will affect the evolutionary trajectory of a natural population. In addition to well recognized factors, such as the source of adaptive genetic variation^{11,12} and the scenario of environmental change^{12,13}, theoretical studies predict that the number and effect sizes of alleles underlying multi-trait adaptive evolution depends on the magnitude of pleiotropy^{14–16}. This relationship was first investigated using Fisher's geometric model, in which every mutation potentially affects all traits. Under this model, the rate of adaptation of an allele should decrease with its degree of pleiotropy¹⁵ owing to the increased probability of antagonistic effects of a mutation when more traits are affected. In other words, the probability that a mutation is advantageous to one trait but detrimental to another trait increases with the degree of pleiotropy, leading to the

concept of the so-called 'cost of complexity'¹⁶. However, in contrast to the assumptions of the geometric model, laboratory studies performed on yeasts, nematodes and mice have found that the degree of pleiotropy follows an L-shaped distribution such that most mutations affect only a small subset of traits^{14,15}. This distribution would diminish the cost of complexity^{15,16}.

Of additional importance is the relationship between the degree of pleiotropy and the per-trait effect size of a mutation (termed pleiotropic scaling)^{14,15}. Most theoretical models assume that the per-trait effect size of a mutation decreases (invariant total-effect model) or remains constant (Euclidean superposition model) with the degree of pleiotropy¹⁶. Laboratory studies, on the other hand, have found synergistic pleiotropy in which the per-trait effect size of a mutation increases with the number of traits affected by that mutation¹⁵. Because this scaling property leads to an increased fitness advantage for more pleiotropic mutations, any cost of complexity is expected to be greatly alleviated¹⁶. Consequently, the combination of restricted and synergistic pleiotropy leads to the prediction that polymorphisms with intermediate degrees of pleiotropy, although rare, should have the highest rate of adaptive evolution^{15,16}. This prediction has not yet been tested empirically.

In its most general sense, pleiotropy refers to the shared impact of polymorphisms. This can include the effect of a polymorphism on (i) multiple phenotypic traits in one environment, referred to as morphological pleiotropy¹⁵; (ii) a single phenotypic trait

¹LIPM, Université de Toulouse, INRA, CNRS, 31326 Castanet-Tolosan, France. ²Laboratoire Evolution, Ecologie et Paléontologie, UMR CNRS 8198, Université de Lille, 59655 Villeneuve d'Ascq Cedex, France. ³INRA, UMR CBGP, 34988 Montferrier-sur-Lez, France. ⁴Institut de Biologie Computationnelle, Montpellier 34095, France. ⁵UMR AGAP, INRA, 34060 Montpellier, France. ⁶INRA, GeT-PlaGe, Genotoul, 31326 Castanet-Tolosan, France. ⁷GenPhySE, Université de Toulouse, INRA, INPT, INP-ENVT, 31326 Castanet-Tolosan, France. ⁸INRA, UAR1209, 31326 Castanet-Tolosan, France. ⁹INRA, UMR1347, Agroécologie, 21065 Dijon, France. ¹⁰Department of Ecology and Evolution, University of Chicago, Chicago, IL 60637, USA. Léa Frachon and Cyril Libourel contributed equally to this work. *e-mail: fabrice.roux@inra.fr

among environments, referred to as environmental pleiotropy¹⁵; or (iii) multiple traits in multiple environments, hereafter called morpho-environmental pleiotropy. Because wild populations evolve in complex abiotic and biotic environments, an exploration of the role of pleiotropy requires consideration of the impact of spatial environmental heterogeneity. In particular, when the same polymorphisms are favoured in distinct micro-habitats, then the suite of selective effects may combine to drive rapid adaptive evolution, whereas competing demands on a polymorphism across micro-sites might inhibit adaptive evolution.

Here, we aimed to generate a comprehensive and unbiased view of how a local population of the annual model plant, *A. thaliana*, changed over an eight-year period in nature. During this time period, our natural population experienced climate change, while it evolved in an environment that is spatially heterogeneous in terms of both biotic and abiotic factors. Therefore, this study adopts the modern standards of ecological genomics to describe the genetic architecture underlying rapid phenotypic evolution of multiple quantitative traits within a local plant population in situ.

Results and discussion

Our study focused on the local population TOU-A (east France; Supplementary Fig. 1) that experienced an increase in mean annual temperature of more than 1°C over the last 30 years (Supplementary Fig. 2). The site occupancy by *A. thaliana* additionally increased between 2002 and 2007 and remained stable thereafter (Supplementary Fig. 1). Seeds of 80 and 115 individual plants (hereafter named accessions) were collected in 2002 and 2010, respectively. Previous studies conducted on accessions collected in 2002 showed that this population has an estimated outcrossing rate of 6% (ref. ¹⁷) and is highly diverse at both genetic (based on genotyping at 149 SNPs) and phenotypic levels^{17–20}. In addition, the TOU-A population presents fine-scale spatial variation for a broad range of soil characteristics and is located between two permanent meadows dominated by grasses (Supplementary Figs. 1, 3).

A resurrection experiment revealed rapid phenotypic evolution. To identify phenotypic traits exhibiting evolutionary change within eight years, we established a resurrection experiment in which the 195 accessions collected in 2002 and 2010 were grown under common environmental conditions. This design enabled us to differentiate plastic from genetic responses²¹. The 195 accessions were grown in situ in six representative micro-habitats, consisting of three contrasting soil types crossed with the presence or absence of the bluegrass *Poa annua*, a species frequently associated with *A. thaliana*²⁰ (Supplementary Fig. 1). A total of 5,850 plants were scored for 29 traits related to phenology, resource acquisition, shoot architecture, seed dispersal, fecundity, reproductive strategy and survival²². Across the six micro-habitats, we detected significant genetic evolution for 16 out of the 29 traits (Fig. 1a and Supplementary Table 1). For example, we found a significant mean delay of 6.1 days for bolting time and a significant mean increase of approximately 7% in the number of fruits produced on the main stem (Fig. 2a). Notably, no evolutionary change was observed for average total seed production across the six micro-habitats, demonstrating that constant seed numbers can be maintained through evolution of flexible life-history and individual reproductive traits. A comparison of our results with the rates of evolution in other plant species²³ suggests a moderate rate of mean phenotypic evolution in the TOU-A population (Fig. 2a).

Analysis of our sequences of the genomes of the 195 accessions (about 25× coverage) confirmed that the mean phenotypic change we observed was not the result of immigration from other phenotypically diverse populations. We observed extensive genetic variation, detecting 1,902,592 SNPs, only 5.6 times less than observed in a panel of 1,135 worldwide accessions²⁴. However, the TOU-A

population appears strongly genetically isolated from other local populations sampled within 1 km (Fig. 3a), confirming the negligible role of immigration in the observed phenotypic change.

Similar phenotypic evolution associated with strong genotype-by-environment interactions. We dissected the phenotypic evolution within each micro-habitat to test whether local abiotic and biotic growing conditions affect the genotype–phenotype relationships in the TOU-A population. Across the 29 traits measured in the six micro-habitats, 144 of the 174 eco-phenotypes displayed significant genetic variance (Fig. 1b), with broad-sense heritability estimates ranging from 0.20 to 0.87 (mean $H^2 = 0.57$, median $H^2 = 0.60$; Supplementary Table 2). Average values of the phenotypes differed substantially among the six micro-habitats (Fig. 2b and Supplementary Table 1). The proportions (ranging from 22.7% to 76.2%) and identities of genetically variable traits that evolved in our eight-year timespan also depended on the micro-habitat (Figs. 1b, 2c). These results highlight the need to consider fine-scale environmental conditions to obtain an accurate picture of the diversity of micro-evolutionary phenotypic processes occurring within a population.

Although each trait that evolved was consistent in its direction in all micro-habitats (Fig. 1b), we observed highly significant changes in the ranking of accessions among micro-habitats for most traits, with a mean across-micro-habitat genetic correlation of 0.46 (median = 0.46, minimum = 0.04, maximum = 0.89) (Supplementary Table 1 and Supplementary Fig. 4). For example, increased allocation of reproduction to the main stem was consistently observed, but different accessions most strongly manifested this allocation pattern among micro-habitats (Supplementary Fig. 5). These results are in accordance with previous studies revealing genotype-by-environment interactions for plant fitness-related traits at the scale of a few metres^{25,26}. However, the existence of genotype-by-environment interactions does not clarify the extent of pleiotropy governing phenotypes in alternative micro-habitats: phenotypic evolution toward the same optimum may be driven by loci with alleles differing in the magnitude of allelic effects across micro-habitats and/or by distinct genetic bases in different micro-habitats²⁷.

Pleiotropy is restricted and synergistic. To characterize the genetics underlying these environmentally dependent genotype–phenotype relationships, we used genome-wide association (GWA) mapping to determine the genetic architecture, the magnitude of pleiotropy and the extent of pleiotropic scaling. The TOU-A population is well-suited for GWA mapping, because it is phenotypically diverse and linkage disequilibrium decays to $r^2 = 0.5$ within an average of 18 base pairs (Fig. 3b). In agreement with limited linkage disequilibrium, we observed an L-shaped distribution of the size of linkage disequilibrium blocks, with a median size of 780 bp (mean size = 5.5 kb) (Supplementary Fig. 6). To verify our ability to finely map genomic regions associated with phenotypic variation, we first tested for the presence of significant associations of known functional polymorphisms. We successfully identified three known functional genes, conferring either qualitative or quantitative resistance against bacterial pathogens when the 195 TOU-A accessions were infected under controlled conditions. In two out of three cases, the most highly associated SNP (hereafter called top SNP) was located within the gene (*RPS2* and *RKS1*)^{19,28} and in the third case it was located 15 bp away (*RPM1*)²⁹ (Supplementary Fig. 7).

To further assess the efficacy of GWA mapping in the TOU-A population, we followed the methodology used in ref. ³⁰ to calculate enrichments for a priori candidate genes for bolting time in the six in situ micro-habitats (Fig. 1b). Because bolting time is a quantitative trait for which the genetic network has been extensively studied, it is well suited for calculating enrichments for a priori candidate genes. Similar to previous results for a field trial utilizing 197 worldwide accessions³⁰, the enrichment ratio quickly dropped with the

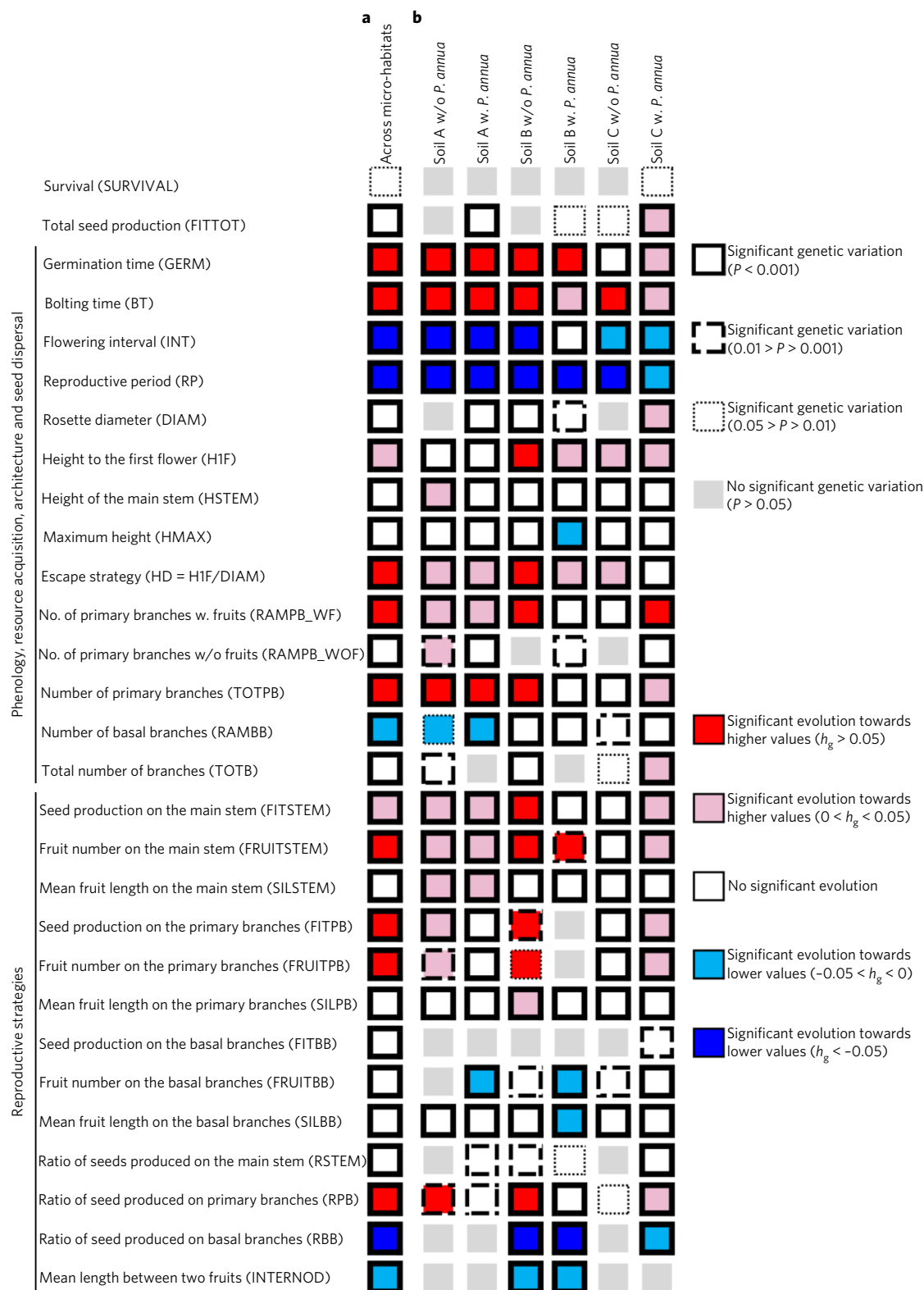


Fig. 1 | Genetic variation among accessions and phenotypic evolution between 2002 and 2010. a, Across the six micro-habitats. Genetic variation was detected for the 29 measured phenotypic traits (mixed model, the term accession was treated as random, $n = 195$). **b**, Within each ‘soil x competition’ micro-habitat (mixed model, the term was accession treated as random, $n = 195$). A, B and C indicate the three types of soil. ‘w/o *P. annua*’ and ‘w. *P. annua*’ correspond to the absence and presence of *P. annua*, respectively. The number of genetically variable traits varied between 21 (soil A in the absence of *P. annua*) and 28 (soil C in the presence of *P. annua*). The percentage of evolved genetically variable traits varied between 22.7% (soil C in the absence of *P. annua*) and 76.2% (soil A in the absence of *P. annua*). Each genetically variable trait (white and coloured squares) in a given in situ experimental condition was defined as an eco-phenotype ($n = 144$). The rates of evolution are expressed in h_g , which corresponds to a metric that scales the magnitude of change by incorporating trait standard deviations ($n = 195$ accessions, 95% confidence intervals obtained by bootstrapping 1,000 random samplings with replacement of genetic values within each year).

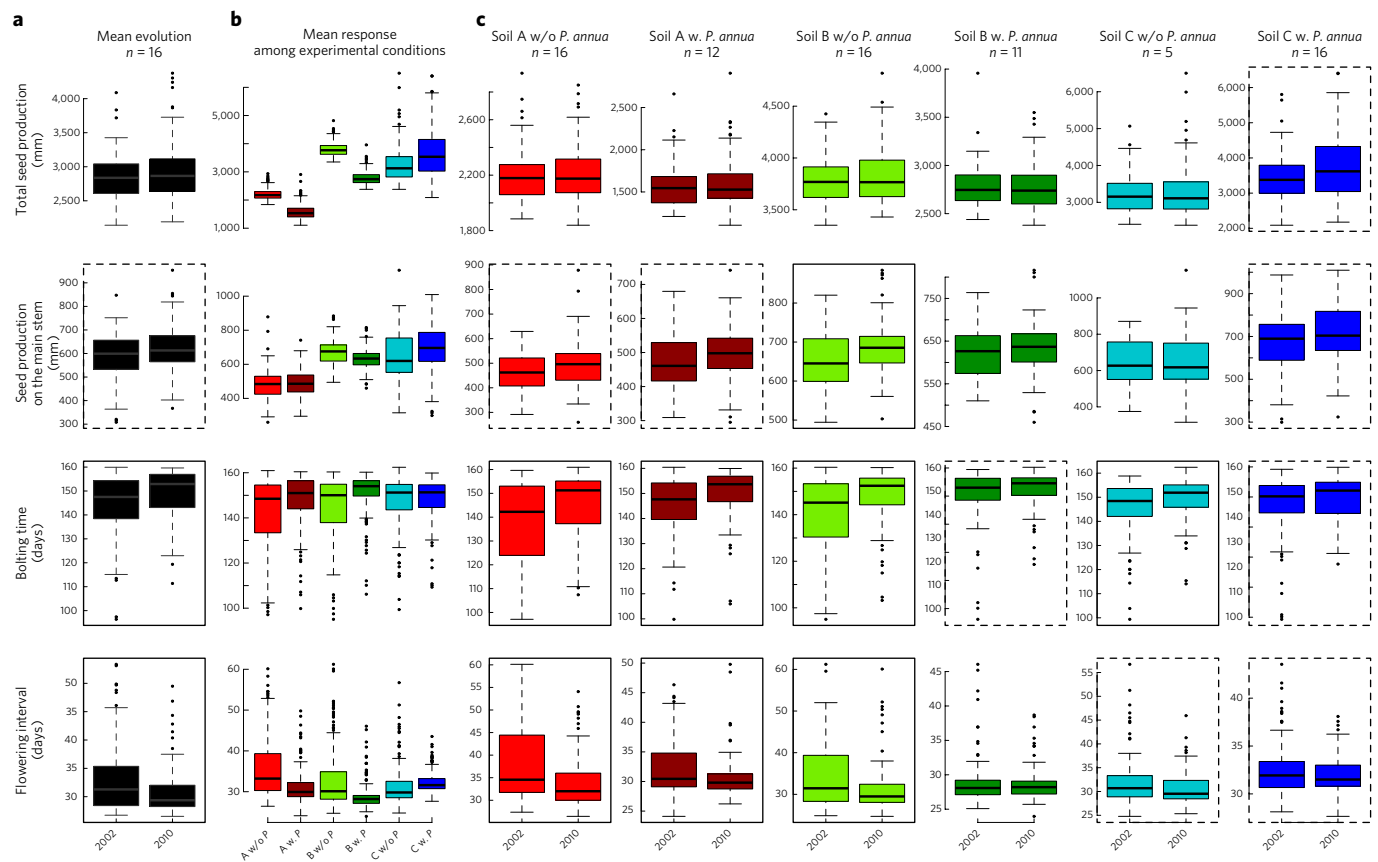


Fig. 2 | Phenotypic changes in the TOU-A population over eight generations. **a**, Mean phenotypic evolution across the six micro-habitats. The total number of seeds produced can be maintained through evolution of phenological (bolting time and flowering interval) and individual reproductive (seed production on the main stem) traits. **b**, Comparison among the six in situ soil \times competition micro-habitats. Average values of the phenotypes differed substantially among the six micro-habitats. **c**, Evolution within each in situ micro-habitat. n indicates the number of evolved phenotypic traits (Fig. 1). The identity of genetically variable traits that evolved between 2002 and 2010 depended on the micro-habitat. Each box-and-whisker plot is based on the genotypic values (BLUPs) of the TOU-A accessions (year 2002: $n = 80$; year 2010: $n = 115$). **a–c**, Parameters of the box-and-whisker plots: line, median; box, first to third quartile; upper whisker, third quartile + $1.5 \times$ interquartile range; lower whisker = first quartile – $1.5 \times$ interquartile range. **b,c**, A, B and C indicate the three types of soil. 'w.o P.' and 'w. P.' correspond to the absence and presence of *P. annua*, respectively. **a,c**, Solid and dashed boxes indicate significant evolution with absolute $h_y > 0.05$ and with absolute $h_y < 0.05$, respectively (Fig. 1).

number of top SNPs in five out of six micro-habitats, demonstrating that candidate genes were overrepresented among top-ranking SNPs (Fig. 4a and Supplementary Fig. 8).

Here we illustrate the effects of genetic architecture, magnitude of pleiotropy and pleiotropic scaling when considering the 200 top SNPs (about 0.01% of the total number of SNPs) for each of

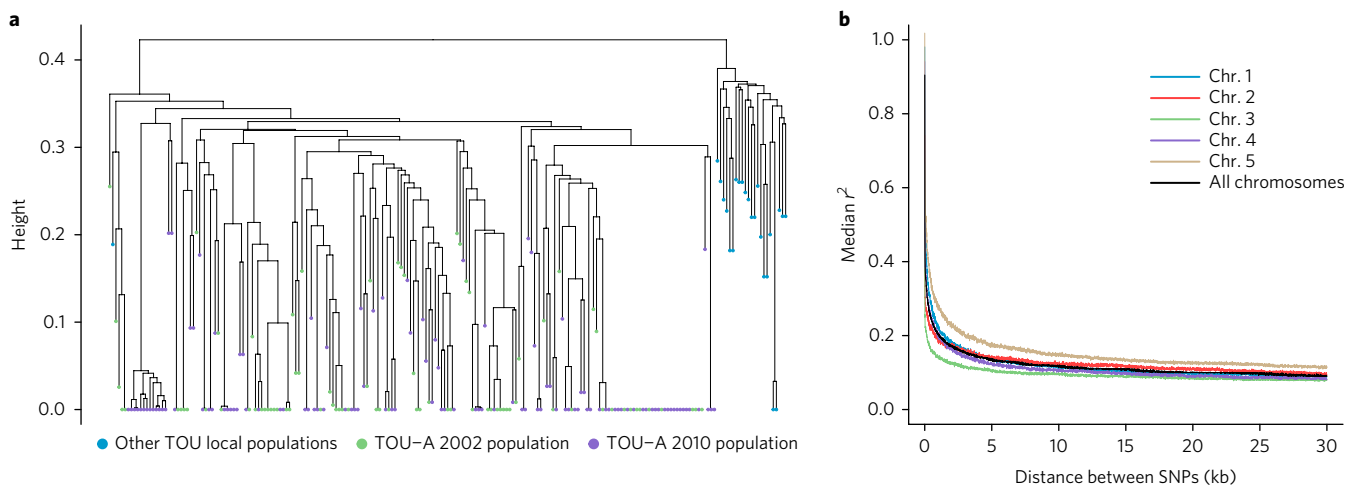


Fig. 3 | Genomic patterns of the TOU-A population. **a**, Hierarchical clustering analysis of the 195 TOU-A accessions and 24 accessions from 10 populations located within 1 km of the TOU-A population. **b**, Decay of linkage disequilibrium (r^2) with physical distance over the five chromosomes of *A. thaliana*.

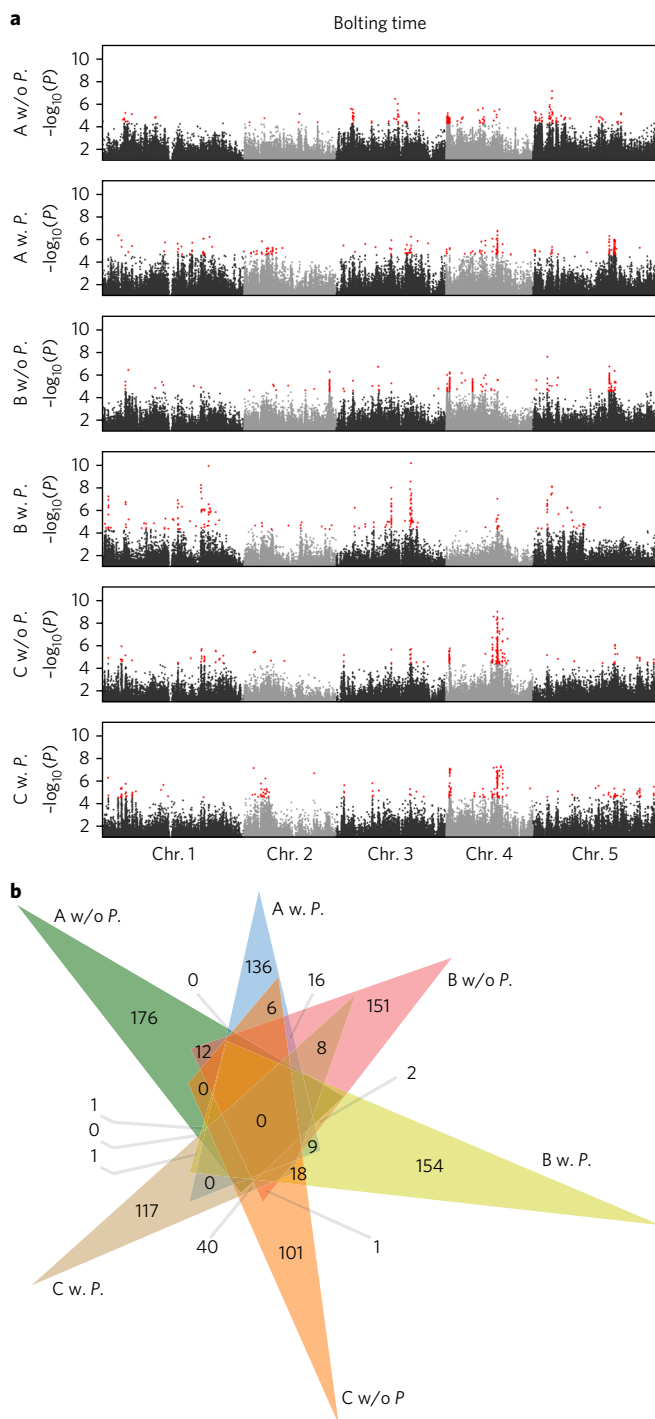


Fig. 4 | Identification of genomic regions associated with bolting time variation in the TOU-A population. a, Manhattan plots of mapping results for each of the six in situ soil \times competition treatments. The x axis indicates the physical position along the chromosome. The y axis indicates the $-\log_{10}(P)$ using the EMMAX method. MARF > 7%. For each experimental condition, the 200 top SNPs are highlighted in red. **b**, Venn diagram partitioning the bolting time SNPs detected among the lists of 200 top SNPs for each in situ soil \times competition treatment. Genetic bases underlying bolting time are largely distinct across micro-habitats.

the 144 eco-phenotypes that were heritable. Although we observed significant enrichment for up to the 500 SNPs, the focus on only 200 top SNPs is conservative in defining pleiotropy and increases the

fraction of true positives. Our choice of threshold does not matter: our biological conclusions are robust to successive cutoffs of top SNPs within the range of 50–500 SNPs, and to three successive cutoffs in terms of the significance of SNPs ($-\log_{10}(P) > 6$; $-\log_{10}(P) > 5$; $-\log_{10}(P) > 4$; chosen based on refs^{31–33}).

We first compared the genetic architecture among micro-habitats for GWA results from each of the 144 heritable eco-phenotypes (Supplementary Fig. 9). The number of genes located within 2 kb of the 200 top SNPs ranged from 45 (fruit number on basal branches in soil B with *P. annua*) to 141 (maximum height scored in soil B without *P. annua*) (mean = 105 genes, median = 108 genes; Supplementary Fig. 10). For a given phenotypic trait, the numbers of associated genes and their corresponding allelic effects sometimes varied widely across micro-habitats, even when broad-sense heritabilities were similar (Supplementary Fig. 10 and Supplementary Table 2); for a notable example, see the results for bolting time (Fig. 4a and Supplementary Fig. 11).

The extent of pleiotropy for each top SNP was determined by calculating an effective number of eco-phenotypes, N_{eff} , sharing a given top SNP according to ref.³⁴. This statistic corrects for correlations among eco-phenotypes to produce a measurement of pleiotropy that is not inflated. In agreement with previous laboratory observations in yeasts, nematodes and mice¹⁵, we found that N_{eff} follows an L-shaped distribution (Fig. 5a). More than 78% of top SNPs affected a single trait in a single micro-habitat, indicating that genetic bases are largely distinct across micro-habitats (Supplementary Figs. 12, 13), as illustrated for bolting time (Fig. 4b). As previously noted for yeast, nematode and mouse studies^{14,15}, this pattern of restricted pleiotropy is more consistent with the notion of modular pleiotropy (with mutations in genes being organized into structured networks) than with universal pleiotropy in Fisher's geometric model (that is, each mutation affects every trait)^{15,16}.

Pleiotropic SNPs were most frequently those demonstrating morpho-environmental pleiotropy. In particular, the relative frequency of morpho-environmental pleiotropy increased rapidly with the overall degree of pleiotropy, just as morphological pleiotropy became relatively less common (Supplementary Fig. 14). Perhaps surprisingly, there were very few examples of environmental pleiotropy, in which a significant SNP impacted the same trait in multiple environments. Our observation of the predominance of morpho-environmental pleiotropy is consistent with previous studies in *A. thaliana* reporting that the identity of traits affected by a gene can depend on the abiotic and biotic phenotyping environment^{35,36} and highlights the importance of spatial environmental heterogeneity in determining the role of pleiotropy on phenotypic evolution of a suite of quantitative traits.

We found that the total-effect size of a top SNP, calculated by either the Manhattan distance (T_M) or the Euclidean distance (T_E), increased with N_{eff} faster than linearly ($T_M = cN_{\text{eff}}^d$, $d = 1.226 \pm 0.003$; $T_E = aN_{\text{eff}}^b$, $b = 0.724 \pm 0.0035$; Fig. 5b, Supplementary Figs. 13, 15 and Supplementary Tables 3, 4). This empirical pattern of synergistic pleiotropy contrasts with most theoretical models, which typically assume that the per-trait effect size of a mutation decreases ($d = 0.5$ or $b = 0$, invariant total-effect model) or remains constant ($d = 1$ or $b = 0.5$, Euclidean superposition model) with the degree of pleiotropy¹⁶. While previously observed in controlled laboratory conditions¹⁵, our study reveals that such a pattern of synergistic pleiotropy can also extend to phenotypes scored in ecological realistic conditions. It should be noted that the non-linear relationship between total-effect size and degree of pleiotropy is robust to successive decreasing cutoffs of N_{eff} (Supplementary Table 5), suggesting that the pattern of synergistic pleiotropy detected in our study is not driven solely by highly pleiotropic SNPs.

Intermediate degrees of synergistic pleiotropy drive adaptive evolution. According to theoretical predictions^{15,16}, the combination of

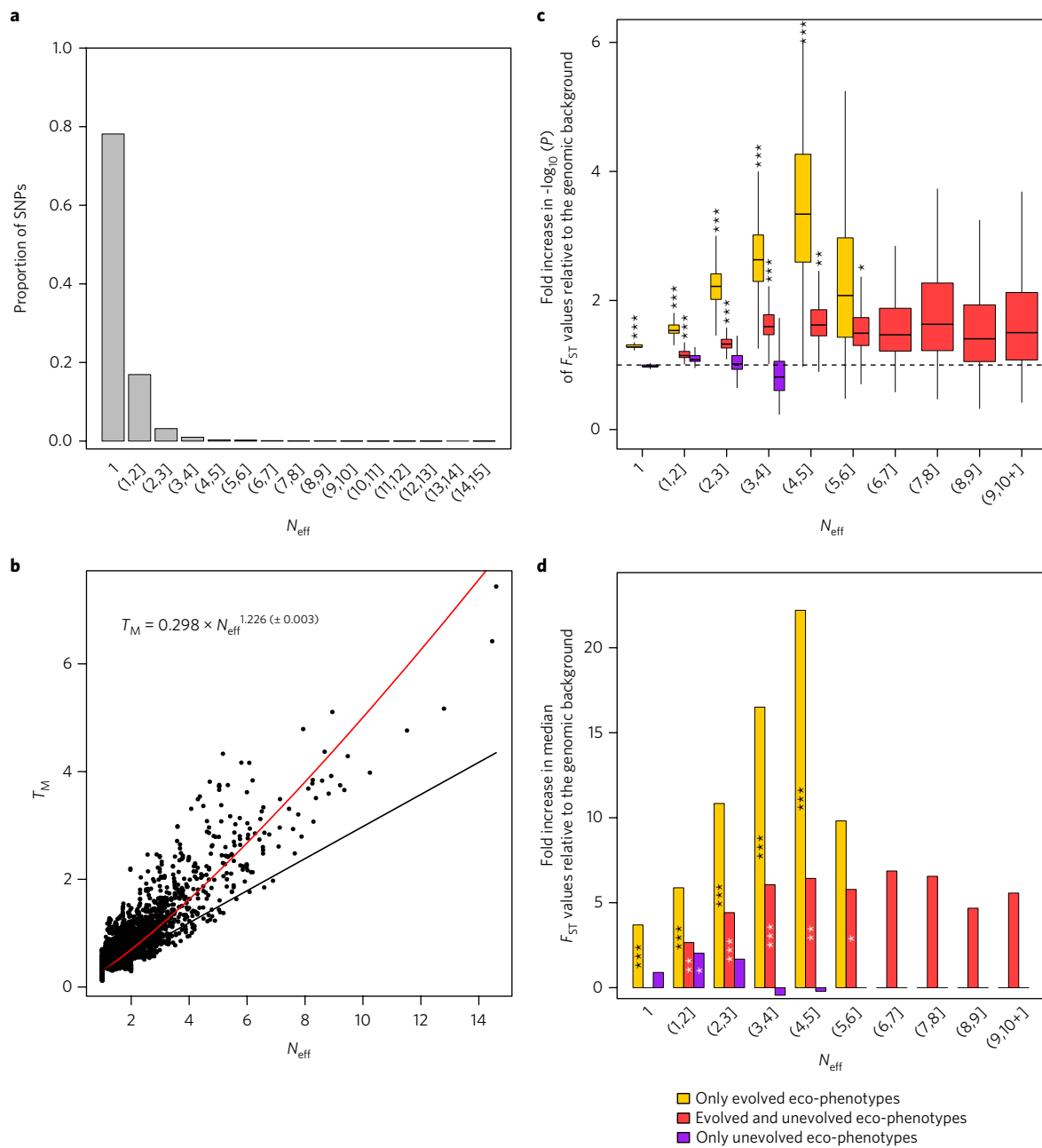


Fig. 5 | Genetic architecture underlying in situ phenotypic evolution in the TOU-A population when considering a threshold of 200 top SNPs.

a, Frequency distribution of the effective number of eco-phenotypes affected by a SNP (N_{eff} , accounting for the correlations among eco-phenotypes)³⁴ among the 21,268 unique top SNPs. **b**, Regression of total-effect size T_M (calculated by the Manhattan distance) on N_{eff} . The formula corresponds to the pleiotropic scaling relationship $T_M = cN_{\text{eff}}^d$. A scaling component d greater than 1 indicates that the mean per-trait effect size of a given top SNP increases with N_{eff} (refs^{14,15}). Solid red line: fitted relationship between T_M and N_{eff} ; solid black line: linear dependence ($d=1$). **c**, Fold increase in median $-\log_{10}(P)$ of neutrality tests based on temporal differentiation for SNPs that hit only evolved eco-phenotypes, only unevolved eco-phenotypes or both types of eco-phenotype, according to different classes of effective number of eco-phenotypes. Parameters of the box-and-whisker plots: line, median; box, first to third quartile; upper whisker, third quartile + 1.5 × interquartile range; lower whisker = first quartile – 1.5 × interquartile range. The dashed line corresponds to a fold increase of 1, that is, no increase in median significance of neutrality tests based on temporal differentiation. **d**, Fold increase in median F_{ST} values for SNPs that hit only evolved eco-phenotypes, only unevolved eco-phenotypes or both types of eco-phenotype, according to different classes of N_{eff} (median F_{ST} across the genome = 0.00293). Significance against a null distribution obtained by bootstrapping: * $0.05 > P > 0.01$, ** $0.01 > P > 0.001$, *** $P < 0.001$, absence of symbols: not significant.

an L-shape distribution of N_{eff} and synergistic pleiotropy should lead polymorphisms with intermediate degrees of pleiotropy, although rare, to experience the highest rates of adaptive evolution. One approach for determining rates of adaptive evolution is to measure the fitness impact of particular SNPs in particular environments.

Unfortunately, the fitness proxies that we measured (for example, total seed production and survival) were not genetically variable in some micro-habitats (Fig. 1b). This does not imply an absence of additive genetic variance for fitness, because we did not measure key germination and seedling survival traits. Therefore, we instead

estimated signatures of selection on top SNPs by testing for the homogeneity of differentiation across SNP markers between our two temporal samples. Such a population genomics approach allows taking into account both the effect of selective processes at all life-stages and the effect of local demographic history between 2002 and 2010.

A genome-wide scan for selection based on temporal differentiation (F_{ST}) (Supplementary Fig. 16) revealed a signature of selection for top SNPs associated with evolved eco-phenotypes, but not for top SNPs associated with unevolved eco-phenotypes; top SNPs jointly associated with evolved and unevolved eco-phenotypes revealed an intermediate signature of selection (Fig. 5c and Supplementary Fig. 13). Because temporal differentiation was tested against changes in the genomic background, this result rejects the hypothesis of selectively neutral evolution for evolved eco-phenotypes. When focusing on top SNPs associated with evolved eco-phenotypes, we found that single-trait micro-habitat-specific SNPs were weakly differentiated, whereas SNPs exhibiting an intermediate degree of pleiotropy revealed the largest fold increase in median temporal F_{ST} values (Fig. 5d and Supplementary Fig. 13). This pattern is strengthened when considering only the top SNPs for evolved phenotypes that have a polarity of effects in line with the direction of phenotypic evolution (around 75.4% of the total number of top SNPs associated with evolved eco-phenotypes; Supplementary Fig. 17). In addition, we found that the mean F_{ST} value of the top SNPs was significantly and positively associated with the rates of phenotypic evolution when we considered the evolved eco-phenotypes, but not when we considered the unevolved eco-phenotypes (Supplementary Fig. 18). Taken together, and considering the prevalence of morpho-environmental pleiotropy observed at intermediate degrees of pleiotropy (Supplementary Fig. 14), our results suggest the evolution of a common adaptive strategy that was accelerated owing to top SNPs being shared across environments, although they affect different traits in different environments.

As previously highlighted for the patterns of restricted pleiotropy and synergistic pleiotropy, the relationships between the degree of pleiotropy and signatures of selection were robust to the different number of top SNPs and thresholds of significance (within the range considered; Supplementary Fig. 13).

Identity of candidate genes under directional selection. The most pleiotropic genes underlying adaptive evolution in the TOU-A population were determined by retrieving all genes associated with 11 or more evolved eco-phenotypes. Among the 14 candidate genes (Supplementary Table 6), was the floral integrator *TWIN SISTER OF FT* (*TSF*), which was associated with bolting time (three microhabitats), flowering interval (one micro-habitat), the length of reproductive period (three micro-habitats), the number of primary branches (one micro-habitat) and the escape strategy to competition (three micro-habitats). Notably, on the basis of a panel of 948 worldwide accessions of *A. thaliana*, *TSF* has been found to be significantly associated with climate variation (that is, the number of consecutive cold days)³⁷, suggesting that *TSF* may have a major role in the adaptation of *A. thaliana* to climate at different geographical scales.

We additionally tested for biological processes that were enriched in the extreme tail of our genome-wide temporal differentiation scan (Supplementary Table 7). In total, 24 biological processes were enriched, 15 of which were supported by genes associated with phenotypic traits measured in this study (Supplementary Table 7). Enrichment for vernalization response was supported by *VERNALIZATION2* (*VRN2*), associated with six eco-phenotypes including two proxies of fitness (that is, survival and seed production; Supplementary Table 7). We also detected many related, enriched functions such as stamen development, pollen maturation and callose deposition (Supplementary Table 7), these are consistent with the simultaneous evolution of fecundity traits observed in this study (Fig. 1). For instance, the candidate gene *POWDERY*

MILDEW RESISTANT 4 is traditionally regarded as a defense response to wounding and pathogens owing to its role in reinforcing the cell wall, although it is also essential for pollen viability and cell division³⁸. In this study, *POWDERY MILDEW RESISTANT 4* was associated with two fecundity traits: mean fruit length on primary branches (in soil A without *P. annua*) and the number of fruits on the main stem (in soil C with *P. annua*; Supplementary Table 7). The simultaneous evolution of fecundity traits suggests an adaptive strategy of short-lived semelparous species such as *A. thaliana* in crowded environments, where plants tend to escape competition^{20,39}. In agreement with this hypothesis, we observed an evolution of an escape strategy trait in five out of six micro-habitats (Fig. 1b).

The remaining nine enriched biological processes were supported by genes that were not associated with any measured phenotype. This is not surprising, in that we missed the entire seed and seedling stage, and did not capture the entire suite of biotic and abiotic factors that can affect selection over time. Among these candidate genes was the MADS-box transcription factor *FLOWERING LOCUS C* (*FLC*) that, in agreement with the recent local warming experienced by the TOU-A population, supported the strong enrichment detected for vernalization response, response to temperature stimulus and regulation of circadian rhythm (Supplementary Table 6). *FLC* is a well-known pleiotropic gene⁴⁰ that affects many traits that we did not measure (such as vernalization response, water-use efficiency and regulation of seed dormancy by maternal temperature)^{41–44}, suggesting that one or more of these traits may have undergone contemporary and rapid phenotypic evolution in the TOU-A population. For example, the proportion of accessions with a slow rather than rapid vernalization haplotype at *FLC*⁴² increased between 2002 and 2010 (χ^2 test = 16.554, $P = 0.000047$; Supplementary Fig. 19). Such a pattern is understandable in light of the increase in the number of chilling degree days observed between 2002 and 2010 (Supplementary Fig. 2).

It is interesting to note that we identified two central regulators of flowering time in our set of candidate genes, that is, *FLC* and *TSF*. In two *Brassica rapa* populations that evolved rapidly following drought in Southern California¹⁰, rapid evolution was in part mediated by a homologue of *SUPPRESSOR OF OVEREXPRESSION OF CONSTANS 1* (*SOC1*), a target of *FLC*-mediated transcriptional repression⁴⁵, suggesting that central regulators of flowering time have a major role in the response to global warming.

Conclusion

Our ecological genomic comparison of plants separated by eight generations revealed rapid multi-trait adaptive evolution that was similar among six micro-habitats, but largely mediated by different genes. The strong genotype-by-environment interactions highlight the importance of considering fine-scale ecological variation. By limiting the erosion of standing genetic variation, this micro-habitat-dependent genetic architecture should allow populations like TOU-A to continue to respond to future environmental changes.

In addition, the combination of GWA studies and an in situ resurrection experiment validated the prediction that polymorphisms with intermediate degrees of pleiotropy, although rare, should have the highest rate of adaptive evolution. This result reinforces the importance of simultaneous evolution of multiple traits in shaping the genomic adaptive trajectory of natural populations. On-going resurrection projects in plants⁴⁶ and long-term population surveys of wild animals⁴⁷ represent an exciting opportunity to test whether restricted pleiotropy combined with synergistic pleiotropy also underlies contemporary and rapid adaptive evolution in other plant and animal species.

Methods

Plant material. The population TOU-A is located under a 350-m electric fence separating two permanent meadows experiencing cycles of periodic grazing by

cattle in the village of Toulon-sur-Arroux (France, Burgundy, 46° 38' 57.302" N, 4° 7' 16.892" E). Seeds from individual plants were collected in 2002 (TOU-A-2002, $n=80$) and 2010 (TOU-A-2010, $n=115$) according to a sampling scheme allowing us to take into account the density of *A. thaliana* plants along a 350-m transect (Supplementary Fig. 1). Differences in maternal effects among the 195 accessions collected in 2002 and 2010 were reduced by growing one plant per family under controlled greenhouse conditions, for one generation (16-h photoperiod, 20 °C).

Ecological characterization. Eighty-three soil samples collected along the 350-m transect were characterized for 14 edaphic factors¹⁸: pH, maximal water holding capacity (WHC), total nitrogen content (N), organic carbon content (C), C/N ratio, soil organic matter content (SOM), concentrations of P₂O₅, K, Ca, Mg, Mn, Al, Na and Fe. Climate data were generated with the ClimateEU v.4.63 software package⁴⁸.

Phenotypic characterization. An experiment of 5,850 plants was set up at the local site of the TOU-A population. The 195 accessions collected in 2002 and 2010 were grown in six representative 'soil × competition' micro-habitats. Each of these micro-habitats was organized in five blocks. Each of the five blocks corresponded to an independent randomization of 195 plants with one replicate per accession collected in 2002 and 2010. Seeds were sown in late September to mimic the main natural germination cohort observed in the TOU-A population (Supplementary Fig. 1). Each plant was scored for a total of 29 phenotypic traits chosen to characterize the life history of *A. thaliana*, including the timing of offspring production or seed dispersal, or because they are involved in the response to competition and/or are good estimators of life-time fitness and reproductive strategies²².

Phenotypic analyses, natural variation, phenotypic evolution and evolutionary rates. We analysed natural variation of all phenotypic traits using the following statistical mixed model:

$$Y_{ijklm} = \mu_{\text{trait}} + \text{block}_k(\text{soil}_i, \text{comp}_k) + \text{soil}_i + \text{comp}_k + \text{soil}_i \text{comp}_k + \text{year}_j + \text{soil}_i \text{year}_j + \text{comp}_k \text{year}_j + \text{soil}_i \text{comp}_k \text{year}_j + \text{accession}_m(\text{year}_j) + \text{accession}_m(\text{year}_j) \text{soil}_i + \text{accession}_m(\text{year}_j) \text{comp}_k + \text{accession}_m(\text{year}_j) \text{soil}_i \text{comp}_k + \varepsilon_{ijklm} \quad (1)$$

In this model, Y is one of the 29 phenotypic traits, μ is the overall phenotypic mean; block accounts for differences between the five experimental blocks within each type of soil × absence or presence of *P. annua* experimental combination; soil corresponds to the effects of the three types of soil; comp measures the effect of the presence of *P. annua*; year corresponds to the effect of the two sampling years 2002 and 2010; accession measures the effect of accessions within each year; interaction terms involving the accession term account for genetic variation in reaction norms of accessions between the three types of soil and the absence or presence of *P. annua*; and ε is the residual term.

All factors were treated as fixed effects, except accession, which was treated as a random effect. For fixed effects, terms were tested over their appropriate denominators for calculating F values. Significance of the random effects was determined by likelihood ratio tests of the model with and without these effects. When necessary, raw data were either log-transformed or Box-Cox transformed to satisfy the normality and equal variance assumptions of linear regression. A correction for the number of tests was performed for each modelled effect to control the false discovery rate (FDR) at a nominal level of 5%.

Inference was performed using REML estimation, using the PROC MIXED procedure in SAS v.9.3 (SAS Institute Inc., Cary, North Carolina, USA) for all traits with the exception of survival, which was analysed using the PROC GLIMMIX procedure in SAS v.9.3.

For all traits, best linear unbiased predictions (BLUPs) were obtained for each accession in each of the six experimental conditions, using the PROC MIXED procedure in SAS v.9.3:

$$Y_{imc} = \mu_{\text{trait}} + \text{block}_k + \text{accession}_m + \varepsilon_{im} \quad (2)$$

For each trait, significant genetic variation among the accessions was detected by testing the significance of the accession term in equation (2). A correction for the number of tests was performed for the modelled accession effect (across the 29 traits within each of the six experimental conditions) to control the FDR at a nominal level of 5%. Because *A. thaliana* is a highly selfing species¹⁷, BLUPs correspond to the genotypic values of accessions.

In each of the six experimental conditions, rates of evolutionary change based on genotypic values of accessions were calculated in haldanes (h_g) for all eco-phenotypes with significant genetic variation among the 195 accessions collected in 2002 and 2010. h_g is a metric that scales the magnitude of change by incorporating trait standard deviations^{49,50}. h_g values were calculated between 2002 and 2010, as:

$$h_g = \frac{(x_2/s_p) - (x_1/s_p)}{g} \quad (3)$$

where x corresponds to the mean genotypic value at year 1 (TOU-A population collected in 2002) and year 2 (TOU-A population collected in 2010), s_p is the standard deviation of the genotypic values of the trait pooled across the two years, and g is the number of generations. Because only one germination cohort was observed every year between 2002 and 2010 (that is, fall germination cohort), only one generation per year was considered in the calculation of h_g values. For a given trait, 95% confidence intervals were estimated based on the distribution of 1,000 h_g values obtained by bootstrapping 1,000 random samplings with replacement of genetic values within each year. A h_g value was considered significantly different from zero if its 95% confidence intervals did not overlap zero.

Sequencing and polymorphism detection. DNA-sequencing experiments were performed on an Illumina HiSeq2500 using a paired-end read length of 2 × 100 pb with the Illumina TruSeq SBS v.3 Reagent Kits. Raw reads of each of the 195 accessions were mapped onto the TAIR10 *A. thaliana* reference genome Col-0 with a maximum of 5 mismatches on at least 80 nucleotides. A semi-stringent SNP calling across the genome was then performed for each accession with SAMtools mpileup (v.0.0.1019)⁵¹ and VarScan (v.2.3)⁵² with the parameters corresponding to a theoretical sequencing coverage of 30× and the search for homozygous sites.

Patterns of linkage disequilibrium and geographic structure. Considering only SNPs with a minor allele relative frequency (MARF) > 0.07, the extent of linkage disequilibrium within 30-kb windows on each chromosome were estimated using VCFtools⁵³. Linkage disequilibrium blocks across the genome were identified in the PLINK environment using the following parameters: --blocks no-pheno-req --maf 0.07 --blocks-max-kb 200, leading to the identification of 19,607 blocks with at least two SNPs (mean number of SNPs per block = 47.6, median number of SNPs per block = 12, mean block length = 5.5 kb, median block length = 0.78 kb). To position the TOU-A population within the local geographic structure, we retrieved the positions of the 214,051 SNPs genotyped on 24 accessions from 10 populations located within 1 km of the TOU-A population²³ across the genomes of the TOU-A population. Clustering genotype analysis was performed using the packages gdsfmt and SNPRelate in the R environment⁵⁵, using the snpGdistLD pruning command with the following parameters: ld.threshold = 0.8 slide.max.bp = 500 maf = 0.07, leaving us with 90,883 SNPs.

GWA mapping and MARF threshold. GWA mapping was run using a mixed-model approach implemented in the software EMMAX (Efficient Mixed-Model Association eXpedited)⁵⁶. This model includes a genetic kinship matrix as a covariate to control for population structure.

Because of bias due to rare alleles^{30,56,57}, we estimated a MARF threshold above which the P -value distribution is not dependent on the MARF. We plotted the 99% quantile of the P -value distribution of all 144 eco-phenotypes (that is, 'micro-habitat × trait' combinations) displaying significant genetic variance (Fig. 1) along 50 MARF values (with an increment of 0.01 from 0.01 to 0.5). A locally weighted polynomial regression indicated that P -value distributions were dependent on MARF value. From visual inspection, we considered a threshold of MARF > 0.07, which resulted in a total of 981,617 SNPs for the subsequent analyses (Supplementary Fig. 20).

Enrichment for a priori candidate genes. To determine the threshold number of top SNPs (that is, SNPs with the highest associations) above which additional top SNPs would behave like the rest of the genome, we calculated enrichments for a priori candidate genes for natural genetic variation of bolting time observed in the six in situ experimental conditions (Fig. 1). On the basis of an algorithm described in ref. 30 and a list of 328 candidate genes for bolting time¹⁸, enrichment was calculated for progressively fewer selective sets of top SNPs within a 20-kb window of an a priori candidate gene. For each set of top SNPs, a null distribution of enrichment was computed to determine a 95% confidence interval³⁰.

Degree of pleiotropy and pleiotropic scaling. Each trait displaying significant genetic variance in a given in situ micro-habitat was considered an eco-phenotype. The degree of pleiotropy of a given top SNP was defined as the number of eco-phenotypes that shared this top SNP. To account for the correlations between eco-phenotypes that can overestimate the degree of pleiotropy, we followed ref. 14 by estimating for each top SNP an effective number of eco-phenotypes as $N_{\text{eff}} = N - \text{var}(\lambda)$ where $\text{var}(\lambda)$ is the variance of the eigenvalues of the error-corrected matrix.

The allelic effects were calculated using the mixed model implemented in the software EMMAX after fitting the pairwise genetic kinship effect⁵⁶. Because different units were used to measure the 29 traits scored in this study, we calculated a standardized allelic effect for each eco-phenotype affected by a top SNP according to ref. 14. The standardized effect on eco-phenotype i , denoted by A_i , is half the difference in genotypic means between the two homozygous genotypes. The total size of the phenotypic effects of a top SNP was then calculated by the Manhattan distance⁵⁸ $T_M = \sum_{i=1}^n |A_i|$ where n is the degree of pleiotropy and A_i is the standardized allelic effect¹⁴⁻¹⁶. The pleiotropic scaling relationship between the total effect size and the effective number of eco-phenotypes was calculated as $T_M = cN_{\text{eff}}^d$.

The pleiotropic scaling relationship between the total-effect size and the effective number of eco-phenotypes was also calculated as $T_E = aN_e^{b_i}$ with T_E corresponding to the Euclidean distance and calculated as $T_E = \sqrt{\sum_{i=1}^n A_i^2}$ where n is the degree of pleiotropy and A_i is the standardized allelic effect.

The degree of pleiotropy and the pleiotropic scaling relationship were calculated for five thresholds of top SNPs (that is, 50 SNPs, 100 SNPs, 200 SNPs, 300 SNPs and 500 SNPs) and three thresholds of significance ($-\log_{10}(P) > 6$, $-\log_{10}(P) > 5$, $-\log_{10}(P) > 4$). To avoid pseudo-replication due to the presence of several top SNPs in a given linkage disequilibrium block ($n = 19,607$ blocks with at least two SNPs), the pleiotropic scaling was also calculated for each threshold number of top SNPs and each threshold of significance by considering the mean value of T_M (or T_E) and N_{eff} per linkage disequilibrium block containing top SNPs and by randomly sampling one top SNP per linkage disequilibrium block (this step was repeated 1,000 times).

Genome-wide scan for selection based on temporal differentiation. In the following, we outline a procedure based on ref. ⁵⁰ to test for the homogeneity of differentiation across SNP markers between two temporal samples. If all SNP markers are selectively neutral, they should provide estimates of temporal differentiation drawn from the same distribution, which depends on the strength of genetic drift in the population (and therefore on its effective size). By contrast, if some marker loci are targeted by selection (or if they are in linkage disequilibrium with selected variants), then some heterogeneity in locus-specific measurements of temporal differentiation should be observed. This is due to selection that will tend to drive measurements of differentiation to values greater (or smaller) than expected under drift alone. The rationale of our approach is therefore to identify those SNPs that show outstanding differentiation, compared to the neutral expectation.

We measured temporal differentiation between sample pairs using F_{ST} . Although the F_C statistic⁶⁰ was used in ref. ⁵⁹, estimators of F_{ST} have better statistical properties in terms of bias and variance, and multilocus estimates have been precisely defined and thoroughly evaluated⁶¹.

Using a multilocus estimate of F_{ST} from the pair of temporal samples, we infer the effective size of the population. Because the 195 *A. thaliana* accessions are considered highly homozygous across the genome, heterozygous sites were discarded (see above) and the data therefore consist of haploid genotypes. We considered a single haploid population of constant size N_e , which has been sampled at generation 0, and τ generations later. Generations do not overlap. New mutations arise at a rate μ , and follow the infinite allele model (IAM). Following ref. ⁶², the pairwise parameter F_{ST} between the two samples can be calculated: $F_{ST} = \frac{1 - e^{-\theta T/2}}{1 + \theta - e^{-\theta T/2}}$ where $T \equiv \tau / N_e$ and $\theta \equiv 2N_e\mu$. In the low mutation limit (that is, as $\mu \rightarrow 0$):

$$F_{ST} \approx \frac{T}{T+2} = \frac{\tau}{\tau + 2N_e}$$

This suggests that a simple moment-based estimator of effective population size can be derived as:

$$\hat{N}_e = \frac{\tau(1 - \hat{F}_{ST})}{2\hat{F}_{ST}}$$

where \hat{F}_{ST} is a multilocus estimate of the parameter F_{ST} . In subsequent analyses, we use the estimator of ref. ⁶¹, preliminary analyses showed that these estimates of effective size have a lower bias and variance than averaged estimates based on single-locus estimates of F_C .

In this study, the pairwise differentiation between the 195 *A. thaliana* accessions samples collected in 2002 and 2010 based on the full set of 1,902,592 SNP markers was: $\hat{F}_{ST} = 0.0215$, which gives an estimate of $\hat{N}_e = 182$ (measured as a number of gene copies).

For each SNP, we tested the null hypothesis that the locus-specific differentiation measured at this focal marker was only due to genetic drift. For this purpose, we computed the expected distribution of F_{ST} for each SNP, conditional upon the estimated effective size (using the same estimated value for all markers: $\hat{N}_e = 182$), and the allele frequencies at the focal SNP in the initial sample (that is, 80 accessions collected in 2002). We simulated individual gene frequency trajectories, as follows.

Suppose that we observe k_0 copies of the reference allele, out of n_0 sampled genes, in the 2002 sample. We assume that these observed counts are drawn from a binomial distribution $B(n_0, \pi_0)$ where π_0 is the (unknown) allele frequency of the reference allele in the population. Assuming a $\beta(1, 1)$ prior distribution for π_0 (uniform distribution), and using the Bayes inversion formula, the posterior distribution of π_0 is a $\beta(k_0 + 1, n_0 - k_0 + 1)$. For each marker and for each simulation, we therefore draw the initial allele frequency $\tilde{\pi}_0$ from a $\beta(k_0 + 1, n_0 - k_0 + 1)$. We then draw 'pseudo-observed' allele counts using a random draw from $B(n_0, \tilde{\pi}_0)$. This procedure allows accounting for the sampling variance in initial allele frequencies, instead of fixing $\tilde{\pi}_0$ to the observed frequency in the sample, as has previously been done⁵⁹.

Then we simulated eight generations of drift, using successive binomial draws with parameters $\hat{N}_e = 182$ and the allele frequency in the previous

generation. In the last generation, a sample of genes is taken as a binomial draw with parameters n_t (the sample size in 2010) and $\tilde{\pi}_t$ (the simulated allele frequency in the last generation).

Next we computed locus-specific estimates of temporal F_{ST} from the simulated allele counts at the initial and last generation. The whole procedure was repeated at least 10,000 times for each marker (additional simulations were performed for some markers to obtain non-null P values).

Finally, we assigned a P value to each SNP marker, computed as the proportion of simulations giving a locus-specific estimate of F_{ST} larger than or equal to the observed value at the focal SNP. We checked that the distribution of P values was fairly uniform (Supplementary Fig. 21).

Note that all SNP markers with a $MARF \leq 0.07$ (computed as the overall frequency across the two temporal samples) were discarded from the analysis. There were 981,617 remaining loci (Supplementary Fig. 16). To avoid any potential bias, all the distributions of F_{ST} were obtained using only simulated markers with a $MARF > 0.07$.

Enrichment analysis of top SNPs for signals of selection. On the basis of the effective number of eco-phenotypes affected by a SNP, we tested whether top SNPs related to evolved eco-phenotypes rejected the hypothesis of selectively neutral evolution more often than top SNPs related to unevolved eco-phenotypes for any given degree of pleiotropy. For each set of top SNPs (that is, top SNPs that hit only evolved eco-phenotypes, top SNPs that hit only unevolved eco-phenotypes and top SNPs that hit both types of eco-phenotypes), we first computed a fold increase in median significance of F_{ST} values using the following ratio: $\text{ratio}_{\text{significance}} = \text{median of } -\log_{10}(P) \text{ of } F_{ST} \text{ values of } n \text{ top SNPs} / \text{median of } -\log_{10}(P) \text{ of } F_{ST} \text{ values of } n \text{ SNPs randomly sampled across the genome}$, where $n =$ number of top SNPs. This step was repeated 1,000 times, generating a distribution of fold increase in median significance of F_{ST} values of top SNPs. We assigned a P value by computing the proportion of $\text{ratio}_{\text{significance}}$ smaller or equal to 1. The random sampling was done according to a scheme that results in sets of SNPs that resemble the original set with respect to linkage disequilibrium³⁷.

We then tested whether the strength of selection differed among the degrees of pleiotropy by computing a fold increase in median F_{ST} values for each set of top SNPs, using the following ratio: $\text{ratio}_{\text{values}} = \text{median of } F_{ST} \text{ values of } n \text{ top SNPs} / \text{median of } F_{ST} \text{ values of all SNPs}$. This step was repeated 1,000 times, by randomly sampling the same number n of SNPs across the genome. This procedure generated a null distribution of fold increase in median F_{ST} values. We assigned a P value by comparing $\text{ratio}_{\text{values}}$ calculated for the set of top SNPs to the quantiles at 95%, 99% and 99.9% of the null distribution.

The enrichment analysis of top SNPs for signals of selection was calculated for five thresholds of top SNPs (that is, 50 SNPs, 100 SNPs, 200 SNPs, 300 SNPs and 500 SNPs) and three thresholds of significance ($-\log_{10}(P) > 6$, $-\log_{10}(P) > 5$, $-\log_{10}(P) > 4$).

Identity of candidate genes under directional selection and enrichment in biological processes. To identify pleiotropic candidate genes associated with the 76 evolved eco-phenotypes, we first selected the 50 SNPs that were the most associated with each evolved eco-phenotype, leading to a total of 3,800 SNPs. We then retrieved all annotated genes located within a 2-kb window on each side of those top SNPs, leading to a final list of 4,855 unique candidate genes. We finally focused on genes associated with 11 or more evolved eco-phenotypes.

To determine which biological processes were important for adaptation of the TOU-A population over eight generations, we tested whether SNPs in the 0.1% upper tail of the F_{ST} distribution were over-represented in each of 736 gene ontology biological processes from the GOSlim set⁶³. For this, 10,000 permutations were run to assess significance using the same methodology as described previously³⁷. For each significantly enriched biological process, we retrieved the identity of all the genes containing SNPs in the 0.1% upper tail of the F_{ST} distribution.

FLC haplotypes analysis. Following ref. ⁴², we extracted the 17 SNPs located within *FLC* and we removed from the analysis 44 accessions with missing information for more than one SNP. We then merged this dataset with the *FLC* SNP dataset obtained across 1,307 accessions of the Regional Mapping panel project^{42,54}. The 17 SNP dataset was used as the input into the software fastPHASE v.1.4.8 (ref. ⁶⁴). fastPHASE was run using the same parameters as described previously⁴² with the exception of invoking the -K20 option to obtain the same number of haplotypes identified in ref. ⁴². We identified eight haplotypes among the 151 TOU-A accessions. Seventy accessions have a haplotype related to a rapid vernalization response (RV haplotype)⁴², whereas 78 accessions have a haplotype related to a slow vernalization response (SV haplotype)⁴². The remaining three accessions are related to an unknown vernalization response profile.

Code availability. Custom scripts developed in this study have been archived in an open access local repository (<https://lipm-browsers.toulouse.inra.fr/pub/Frachon2017-NEE/>). The code for performing genome-wide scan for selection based on temporal differentiation is available from the Zenodo database⁶⁵.

Data availability. The raw sequencing data used for this study are available at the NCBI Sequence Read Archive (<http://ncbi.nlm.nih.gov/sra>) through the study accession [SRP077483](https://doi.org/10.1038/SRP077483).

The phenotypic and genomic files used in this study have been archived in an open access local repository (<https://lipm-browsers.toulouse.inra.fr/pub/Frachon2017-NEE/>).

Received: 15 November 2016; Accepted: 27 July 2017;
Published online: 4 September 2017

References

- Franks, S. J., Weber, J. J. & Aitken, S. N. Evolutionary and plastic responses to climate changes in terrestrial plant populations. *Evol. Appl.* **7**, 123–139 (2014).
- DeLong, J. P. et al. How fast is fast? Eco-evolutionary dynamics and rates of change in populations and phenotypes. *Ecol. Evol.* **6**, 573–581 (2016).
- Buswell, J. M., Moles, A. T. & Hartley, S. Is rapid evolution common in introduced plant species? *J. Ecol.* **99**, 214–224 (2011).
- Franks, S. J., Sim, S. & Weis, A. E. Rapid evolution of flowering time by an annual plant in response to a climate fluctuation. *Proc. Natl Acad. Sci. USA* **104**, 1278–1282 (2007).
- Reid, N. M. et al. The genomic landscape of rapid repeated evolutionary adaptation to toxic pollution in wild fish. *Science* **354**, 1305–1308 (2016).
- van't Hof, A. E., Edmonds, N., Dalikova, M., Marec, F. & Saccheri, I. J. Industrial melanism in British peppered moths has a singular and recent mutational origin. *Science* **332**, 958–960 (2011).
- Hanikenne, M. et al. Evolution of metal hyperaccumulation required cis-regulatory changes and triplication of *HMA4*. *Nature* **453**, 391–395 (2008).
- Délye, C., Jasieniuk, M. & Le Corre, V. Deciphering the evolution of herbicide resistance in weeds. *Trends Genet.* **29**, 649–658 (2013).
- Bay, A. B. et al. Predicting responses to contemporary environmental change using evolutionary response architectures. *Am. Nat.* **189**, 463–473 (2017).
- Franks, S. J., Kane, N. C., O'Hara, N. B., Tittes, S. & Rest, J. S. Rapid genome-wide evolution in *Brassica rapa* populations following drought revealed by sequencing of ancestral and descendant gene pools. *Mol. Ecol.* **25**, 3622–3631 (2016).
- Dittmar, E. L., Oakley, C. G., Conner, J. K., Gould, B. A. & Schmeske, D. W. Factors influencing the effect size distribution of adaptive substitutions. *Proc. R. Soc. B* **283**, 20153065 (2016).
- Matuszewski, S., Hermisson, J. & Kopp, M. Catch me if you can: adaptation from standing genetic variation to a moving phenotypic optimum. *Genetics* **200**, 1255–1274 (2015).
- Kopp, M. & Matuszewski, S. Rapid evolution of quantitative traits: theoretical perspectives. *Evol. Appl.* **7**, 169–191 (2014).
- Wagner, G. P. et al. Pleiotropic scaling of gene effects and the 'cost of complexity'. *Nature* **452**, 470–472 (2008).
- Wang, Z., Liao, B.-Y. & Zhang, J. Genomic patterns of pleiotropy and the evolution of complexity. *Proc. Natl Acad. Sci. USA* **107**, 18034–18039 (2010).
- Wagner, G. P. & Zhang, J. The pleiotropic structure of the genotype–phenotype map: the evolvability of complex organisms. *Nat. Rev. Genet.* **12**, 204–213 (2011).
- Platt, A. et al. The scale of population structure in *Arabidopsis thaliana*. *PLoS Genet.* **6**, e1000843 (2010).
- Brachi, B. et al. Investigation of the geographical scale of adaptive phenological variation and its underlying genetics in *Arabidopsis thaliana*. *Mol. Ecol.* **22**, 4222–4240 (2013).
- Huard-Chauveau, C. et al. An atypical kinase under balancing selection confers broad-spectrum disease resistance in *Arabidopsis*. *PLoS Genet.* **9**, e1003766 (2013).
- Baron, E., Richirt, J., Villoutreix, R., Amsellem, L. & Roux, F. The genetics of intra- and interspecific competitive response and effect in a local population of an annual plant species. *Funct. Ecol.* **29**, 1361–1370 (2015).
- Franks, S. J. et al. The resurrection initiative: storing ancestral genotypes to capture evolution in action. *BioScience* **58**, 870–873 (2008).
- Roux, F. et al. Cytonuclear interactions affect adaptive phenotypic traits of the annual plant *Arabidopsis thaliana* in the field. *Proc. Natl Acad. Sci. USA* **113**, 3687–3692 (2016).
- Bone, E. & Farres, A. Trends and rates of microevolution in plants. *Genetica* **112–113**, 165–182 (2001).
- The 1001 Genomes Consortium. 1,135 genomes reveal the global pattern of polymorphism in *Arabidopsis thaliana*. *Cell* **166**, 481–491 (2016).
- Kalisz, S. Variable selection on the timing of germination in *Collinsia verna* (Scrophulariaceae). *Evolution* **40**, 479–491 (1986).
- Stratton, D. A. Spatial scale of variation in fitness of *Erigeron annuus*. *Am. Nat.* **146**, 608–624 (1995).
- Des Marais, D. L., Hernandez, K. M. & Juenger, T. E. Genotype-by-environment interaction and plasticity: exploring genomic responses of plant to the abiotic environment. *Annu. Rev. Ecol. Syst.* **44**, 5–29 (2013).
- Bent, A. F. et al. *RPS2* of *Arabidopsis thaliana*: a leucine-rich repeat class of plant disease resistance genes. *Science* **265**, 1856–1860 (1994).
- Grant, M. R. et al. Structure of the *Arabidopsis RPM1* gene enabling dual specificity disease resistance. *Science* **269**, 843–846 (1995).
- Brachi, B. et al. Linkage and association mapping of *Arabidopsis thaliana* flowering time in nature. *PLoS Genet.* **6**, e1000940 (2010).
- Van Rooijen, R., Aarts, M. G. M. & Harbinson, J. Natural genetic variation for acclimation of photosynthetic light use efficiency to growth irradiance in *Arabidopsis*. *Plant Physiol.* **167**, 1412–1429 (2015).
- Kooke, R. et al. Genome-wide association mapping and genomic prediction elucidate the genetic architecture of morphological traits in *Arabidopsis*. *Plant Physiol.* **170**, 2187–2203 (2016).
- Thoen, M. P. M. et al. Genetic architecture of plant stress resistance: multi-trait genome-wide association mapping. *New Phytol.* **213**, 1346–1362 (2016).
- Pavlicev, M., Cheverud, J. M. & Wagner, G. P. Measuring morphological integration using eigenvalues variance. *Evol. Biol.* **36**, 157–170 (2009).
- Korves, T. & Bergelson, J. A novel cost of R gene resistance in the presence of disease. *Am. Nat.* **163**, 489–504 (2004).
- Scarcelli, N., Cheverud, J. M., Schall, B. A. & Kover, P. X. Antagonistic pleiotropic effect reduce the potential adaptive value of the FRIGIDA locus. *Proc. Natl Acad. Sci. USA* **104**, 16986–16991 (2007).
- Hancock, A. M. et al. Adaptation to climate across the *Arabidopsis thaliana* genome. *Science* **334**, 83–86 (2011).
- Ellinger, D. & Voigt, C. A. Callose biosynthesis in *Arabidopsis* with a focus on pathogen response: what we have learned within the last decade. *Ann. Bot.* **114**, 1349–1358 (2014).
- Bonsler, S. P. High reproduction efficiency as an adaptive strategy in competitive environments. *Funct. Ecol.* **27**, 876–885 (2013).
- Deng, W. et al. FLOWERING LOCUS C (FLC) regulates development pathways throughout the life cycle of *Arabidopsis*. *Proc. Natl Acad. Sci. USA* **108**, 6680–6685 (2011).
- McKay, J. K., Richards, J. H. & Mitchell-Olds, T. Genetics of drought adaptation in *Arabidopsis thaliana*: I. Pleiotropy contributes to genetic correlations among ecological traits. *Mol. Ecol.* **12**, 1137–1151 (2013).
- Li, P. et al. Multiple FLC haplotypes defined by independent cis-regulatory variation underpin life history diversity in *Arabidopsis thaliana*. *Genes Dev.* **28**, 1635–1640 (2014).
- Blair, L., Auge, G. & Donohue, K. Effect of FLOWERING LOCUS C on seed germination depends on dormancy. *Funct. Plant Biol.* **44**, 493–506 (2017).
- Auge, G. A., Blair, L. K., Neville, H. & Donohue, K. Maternal vernalization and vernalization-pathway genes influence progeny seed germination. *New Phytol.* <http://dx.doi.org/10.1111/nph.14520> (2017).
- Salathia, N. et al. FLOWERING LOCUS C-dependent and -independent regulation of the circadian clock by the autonomous and vernalization pathways. *BMC Plant Biol.* **6**, 10 (2006).
- Etterson, J. R. et al. Project Baseline: an unprecedented resource to study plant evolution across space and time. *Am. J. Bot.* **103**, 164–173 (2016).
- Kruuk, L. E. B., Garant, D. & Charmantier, A. (eds) in *Quantitative Genetics in Wild Populations* 1–15 (Oxford Univ. Press, Oxford, 2014).
- Hamann, A., Wang, T., Spittlehouse, D. L. & Murdock, T. Q. A comprehensive, high-resolution database of historical and projected climate surfaces for western North America. *B. Am. Meteorol. Soc.* **94**, 1307–1309 (2013).
- Hendry, A. P. & Kinnison, M. T. Perspective: the pace of modern life: measuring rates of contemporary microevolution. *Evolution* **53**, 1637–1653 (1999).
- Gingerich, P. D. Rates of evolution on the time scale of the evolutionary process. *Genetica* **112–113**, 127–144 (2001).
- Li, H. et al. The sequence alignment/map format and SAMtools. *Bioinformatics* **25**, 2078–2079 (2009).
- Koboldt, D. C. et al. VarScan 2: somatic mutation and copy number alteration discovery in cancer by exome sequencing. *Genome Res.* **22**, 568–576 (2012).
- Danecek, P. et al. The variant call format and VCFtools. *Bioinformatics* **27**, 2156–2158 (2011).
- Horton, M. W. et al. Genome-wide patterns of genetic variation in worldwide *Arabidopsis thaliana* accessions for the RegMap panel. *Nat. Genet.* **44**, 212–216 (2012).
- Zheng, X. et al. A high-performance computing toolset for relatedness and principal component analysis of SNP data. *Bioinformatics* **28**, 3326–3328 (2012).
- Kang, H. M. et al. Variance component model to account for sample structure in genome-wide association studies. *Nat. Genet.* **42**, 348–354 (2010).
- Atwell, S. et al. Genome-wide association study of 107 phenotypes in *Arabidopsis thaliana* inbred lines. *Nature* **465**, 627–631 (2010).
- Hermisson, J. & McGregor, A. P. Pleiotropic scaling and QTL data. *Nature* **456**, E3–E4 (2008).
- Goldringer, I. & Bataillon, T. On the distribution of temporal variations in allele frequency consequences for the estimation of effective population size and the detection of loci undergoing selection. *Genetics* **168**, 563–568 (2004).

60. Waples, R. S. A generalized approach for estimating effective population size from temporal changes in allele frequency. *Genetics* **121**, 379–391 (1989).
61. Weir, B. S. & Cockerham, C. C. Estimating F -statistics for the analysis of population structure. *Evolution* **38**, 1358–1370 (1984).
62. Skoglund, P., Sjödin, P., Skoglund, T., Lascoux, M. & Jakobsson, M. Investigating population history using temporal genetic differentiation. *Mol. Biol. Evol.* **31**, 2516–2527 (2014).
63. The Gene Ontology Consortium. The Gene Ontology project in 2008. *Nucleic Acids Res.* **36**, D440–D444 (2008).
64. Scheet, P. & Stephens, M. A fast and flexible statistical model for large-scale population genotype data: applications to inferring missing genotypes and haplotypic phase. *Am. J. Hum. Genet.* **78**, 629–644 (2006).
65. Vitalis, R., Gay, L. & Navascues, M. TempoDiff: a computer program to detect selection from temporal genetic differentiation (2017); <https://zenodo.org/record/375600>.

Acknowledgements

We thank B. Brachi for his helpful discussions on the enrichment analysis in biological processes. This work was funded by the Région Midi-Pyrénées (CLIMARES project), the INRA Santé des Plantes et Environnement department (RESURRECTION project), the INRA-ACCAF metaprogram (SELFADAPT project), the LABEX TULIP (ANR-10-LABX-41, ANR-11-IDEX-0002-02) and the National Institute of Health.

Author Contributions

F.R. supervised the project. F.R. conceived and designed the experiments. E.B., L.A., R.Vil. and F.R. conducted the in situ experiment. L.F., C.G., C.H.-C. and F.R. measured the phenotypic traits. L.F. and F.R. analysed the phenotypic traits. O.B. and M.V. generated the sequencing data. S.C. and C.L. performed the bioinformatics analyses. L.F., C.L. and F.R. performed the GWA mapping. L.F., C.L., D.R. and F.R. performed and analysed the enrichment tests. M.N., L.G. and R.Vit. developed a methodology in selfing species to perform a genome-wide scan for selection based on temporal differentiation. V.L.C. and J.B. guided the analysis of phenotypic and genomic data. F.R. and J.B. wrote the manuscript, with contributions from L.F., C.L., R.Vil., M.N., L.G., R.Vit. and D.R. All authors contributed to the revisions.

Competing interests

The authors declare no competing financial interests.

Additional information

Supplementary information is available for this paper at doi:10.1038/s41559-017-0297-1.

Reprints and permissions information is available at www.nature.com/reprints.

Correspondence and requests for materials should be addressed to F.R.

Publisher's note: Springer Nature remains neutral with regard to jurisdictional claims in published maps and institutional affiliations.